Journal of Applied Physics TUTORIAL scitation.org/journal/jap

A first-principles understanding of point defects and impurities in GaN

Cite as: J. Appl. Phys. **129**, 111101 (2021); doi: 10.1063/5.0041506
Submitted: 23 December 2020 · Accepted: 27 February 2021 ·
Published Online: 15 March 2021

John L. Lyons,[1,a)] Darshana Wickramaratne,[1] and Chris G. Van de Walle[2]

AFFILIATIONS

[1]Center for Computational Materials Science, United States Naval Research Laboratory, Washington, DC 20375, USA
[2]Materials Department, University of California, Santa Barbara, California 93106-5050, USA

[a)]**Author to whom correspondence should be addressed:** john.lyons@nrl.navy.mil

ABSTRACT

Attaining control over the electrical conductivity of gallium nitride through impurity doping is one of the foremost achievements in semiconductor science. Yet, unwanted contaminants and point defects continue to limit device performance, and experimental techniques alone are insufficient for elucidating the behavior of these unintentionally incorporated species. Methodological advancements have made first-principles calculations more powerful than ever and capable of quantitative predictions, though care must still be taken in comparing results from theory and experiment. In this Tutorial, we explain the basic concepts that define the behavior of dopants, unintentional impurities, and point defects in GaN. We also describe how to interpret experimental results in the context of theoretical calculations and also discuss how the properties of defects and impurities vary in III-nitride alloys. Finally, we examine how the physics of defects and impurities in GaN is relevant for understanding other wide-bandgap semiconductor materials, such as the II–IV-nitrides, boron nitride, and the transition metal nitrides.

https://doi.org/10.1063/5.0041506

I. INTRODUCTION AND BACKGROUND

GaN is now an essential semiconductor material for applications including blue- and white-light emitting diodes (LEDs), lasers, and power electronics.[1–3] Its ability to be doped both *n*- and *p*-type distinguishes it from most other wide-bandgap semiconductors for which unipolar electrical conductivity is the norm.[4] The development of GaN has relied on advancements in understanding of the role of native defects, unintentional contaminants, and dopant impurities. The breakthrough in achieving *p*-type GaN via magnesium doping[5,6] enabled nitride-based LEDs and laser diodes. However, achieving complete control over Mg-doped material still remains a challenge, for instance, in vertical devices.[7,8] First-principles calculations continue to be a vital means of understanding the properties of dopants and defects in GaN and related materials, such as in describing the properties of newly recognized impurities[9,10] or in identifying detrimental nonradiative recombination centers that could participate in defect-assisted [or Shockley–Read–Hall (SRH)] recombination.[11–14]

Despite its technological importance as a semiconductor, many properties of defects in GaN and its alloys are closer to the behavior in a traditional insulator. For instance, many acceptors exhibit so-called "polaronic" behavior, whereby they trap localized holes, behavior that is usually associated with wide-bandgap insulators.[15] There is a large lattice distortion that accompanies the holes that are trapped due to acceptors in GaN, which leads to broad sub-bandgap luminescence bands. Other properties, such as the *DX* behavior of donors, emerge when GaN is alloyed with the wider-gap AlN. Here, we discuss how the properties of dopants and defects in GaN are driven by these effects, and how first-principles calculations have aided in understanding these behaviors.

Our ability to understand, predict, and control the properties of point defects in GaN has been shaped in large part by advances in the predictive capability of first-principles calculations.[16] Early calculations utilizing density functional theory within the local density approximation (LDA) and the generalized gradient approximation (GGA) were limited by the bandgap problem, which can now be overcome by using hybrid functionals. This has enabled quantitative predictions of the formation energies, thermodynamic transition levels, and the atomic structure of defects. Combined with advances in first-principles methods that address the role of electron–phonon coupling, the accurate calculation of optical transitions,[17,18] radiative[19] and nonradiative[11,20] recombination rates,

temperature dependence of thermodynamic transition levels, and thermal emission rates involving point defects[21] are now possible. These developments are being applied to advance our understanding of point defects in GaN and also to new avenues of research such as the behavior of defects in alloys[22,23] and the role of excited states of defects.[12,13]

This Tutorial is intended to convey the principles behind defect physics in GaN. We attempt to categorize the behavior of different classes of defects, dopants, and impurities and focus on those species that have been most relevant for the development of GaN-based technologies. More extensive reviews of first-principles methodologies for the III-nitrides[24] and for semiconductors in general[16] have been published previously, so we provide here a concise description. For those readers interested in the intersection between theory and experiment, another recent Tutorial[25] discusses approaches to bridge the gap between the theoretical interpretation of experimental measurements. Reviews focused from the experimental standpoint are also available.[26–31]

The structure of this Tutorial is as follows. We begin in Sec. II with a concise description of first-principles defect methodology, focusing on C_N in GaN as a case study. We then discuss effective *n*- and *p*-type dopants in GaN in Sec. III and describe dopants with deep-level characteristics in Sec. IV. Unintentional impurities are reviewed in Sec. V, and the role of native defects is summarized in Sec. VI. Detailed knowledge of defect and impurity behavior in III-nitride alloys is somewhat limited but we cover some recent developments in Sec. VII. We then briefly discuss experimental signatures of defects (and how they can be reconciled with first-principles calculations) in Sec. VIII. We conclude with a discussion on how the principles that govern defect physics in GaN can yield insights into novel nitride materials in Sec. IX.

II. METHODOLOGY OF DEFECT CALCULATIONS

Defect formation energies and transition levels can be calculated within a now well-established formalism.[16] Here, we use the carbon acceptor on the nitrogen site (C_N) as a case study to illustrate such calculations. The formation energy of C_N in charge state q is given by

$$E^f(C_N^q) = E_{tot}(C_N^q) - E_{tot}(GaN) + \mu_N - \mu_C + q(E_F + \varepsilon_v) + \Delta^q, \quad (1)$$

in which $E_{tot}(C_N^q)$ is the total energy of a supercell containing C_N^q in charge state q and $E_{tot}(GaN)$ is the total energy of the same supercell without a defect. An electron added to or removed from the supercell is exchanged with the Fermi level (E_F) of GaN which is referenced to the valence-band maximum (VBM) (ε_v). In a plot of formation energies vs E_F (such as shown in Fig. 2), the VBM is usually at 0 eV on the x axis, and the maximum Fermi level is set to the value of the band gap, which is 3.5 eV for GaN.

Δ^q is a correction term that accounts for finite-size effects that can occur due to using a supercell. As discussed in Refs. 16 and 32, multiple methods are available for obtaining such corrections.[33–35] In our experience, the scheme developed in Refs. 34 and 35, which is based on the explicit treatment of the electrostatic problem, is capable of providing accurate corrections for moderately sized supercells.

The formation energy of a defect will also vary with the chemical potentials of the species involved in creating the defect. Chemical potentials are referenced to the energy of the associated elemental phase [$E(i)$ for species i; for C, this would be the energy of one C atom in the diamond phase] as follows:

$$\mu_i = E(i) + \Delta\mu_i. \quad (2)$$

While $E(i)$ remains constant, $\Delta\mu_i$ is subject to bounds. $\Delta\mu_i$ of the bulk species (i.e., $\Delta\mu_{Ga}$ and $\Delta\mu_N$) are limited by the enthalpy of formation of GaN [ΔH^f(GaN), calculated to be −1.33 eV[36]],

$$\Delta H^f(GaN) = \Delta\mu_N + \Delta\mu_{Ga}. \quad (3)$$

By setting $\Delta\mu_{Ga} = 0$ eV, Ga-rich conditions can be considered; similarly, $\Delta\mu_N = 0$ eV corresponds to N-rich conditions. Secondary phases may further limit the chemical potentials of impurities. For the impurities discussed here, secondary phases are listed in the caption of Fig. 2.

Most defects and dopants can occur in different charge states. C is deficient one electron relative to N, so in the neutral charge state, C_N gives rise to a hole. As we will see in Sec. IV B, such states are derived from C 2*p* orbitals. By adding an electron to fill this hole, we can calculate C_N^-. By removing an electron from C_N^0, a second defect-related hole can be created, stabilizing C_N^+. Which charge state is most stable will depend on the position of E_F. The thermodynamic transition level of a defect (sometimes simply called the "defect level") is defined by the position of the Fermi level where the formation energies of a defect in two different charge states are equal. This quantity is also known as a "defect ionization energy" and describes the electrical behavior of a defect. As will be discussed in Sec. VIII, caution should be exercised when comparing these calculated quantities to experimentally determined values.

C_N gives rise to two thermodynamic transition levels: (+/0) and (0/−). For C_N in GaN, the transition level between charge states 0 and − can be expressed in terms of the formation energies at the VBM (i.e., when E_F=0),

$$(0/-) = E^f(C_N^-; E_F = 0) - E^f(C_N^0; E_F = 0). \quad (4)$$

This level occurs near 1 eV, as shown in Fig. 2. Because this level falls well within the bandgap of GaN, C_N is considered a "deep" defect. Similarly, the transition level between the + and 0 charge states is given by

$$(+/0) = E^f(C_N^0; E_F = 0) - E^f(C_N^+; E_F = 0); \quad (5)$$

it occurs at 0.4 eV above the VBM, as shown in Fig. 2.

If we are in thermodynamic equilibrium (or close to it), the likelihood of incorporation of defects and dopants is determined by their formation energy in the bulk material. However, non-equilibrium factors can play a role in some situations; for instance, surface-dependent adsorption is known to affect nanocrystal doping,[37] and metastable dopant configurations were recently shown to arise from surface adsorption coupled with large migration barriers in $Al_xGa_{1-x}O_3$ alloys.[38] In GaN, surface-dependent

impurity incorporation has been reported[39,40] and may be linked with surface-dependent adsorption.[41] Surface band bending can also play an important role, and such effects have recently been incorporated into first-principles studies.[42] In this Tutorial, we focus on the properties of defects and dopants in thermodynamic equilibrium.

III. SHALLOW DOPANTS

A. Electronic structure of effective-mass dopants

An ideal substitutional donor in GaN would involve replacing either gallium or nitrogen with an element containing extra electrons. Such a donor would also not give rise to defect states within the GaN bandgap, and its extra electron would instead reside at the conduction band minimum (CBM). Binding between the negatively charged electron and positively charged donor would occur through electrostatic interactions, as described by the hydrogenic effective-mass donor model,[43] as depicted in Fig. 1(a). Such binding is weak relative to $k_B T$. This makes for an efficient dopant since the overwhelming majority of such species would be ionized at room temperature.

GaN has a small electron effective mass, meaning there is not a strong driving force for the localization of electron carriers. It also features a relatively low-lying CBM, relative to vacuum, in comparison with other wide-bandgap semiconductors.[44] This means that candidate donors are not likely to give rise to states within the bandgap. Alloying GaN with Al causes an upward relative shift of the CBM and can lead to the appearance of *DX* donor behavior (whereby donor impurities capture electrons to become negatively charged and self compensate). This issue will be discussed in Sec. VII.

As with donor dopants, the ideal substitutional acceptor in GaN would involve replacing Ga or N with an impurity that has one fewer electron and does not give rise to states within the gap. Instead, the resulting hole would reside at the VBM. Ideally, weak binding between the positively charged free hole and the negatively charged acceptor would lead to a small binding energy and hydrogenic acceptor behavior. In GaN, the presence of such hydrogenic acceptor dopants is hindered by two factors: a low-lying valence band and a heavy effective mass. The low-lying VBM causes the atomic orbitals of some potential dopants to reside in the bandgap [giving rise to atomic-like acceptor behavior, analogous to what is shown in Fig. 1(c)], whereas the heavy hole effective mass can lead to hole localization next to acceptors [giving rise to the so-called polaronic acceptor behavior, as depicted in Fig. 1(b)[45]].

A separate concern is that the impurity dopant should incorporate easily into the semiconductor material (i.e., have good solubility). In GaN, this is not a major concern, as the formation energies of common donor and acceptor dopants are low (as will be shown in Fig. 2). Incorporating dopants will lead to a shift in the Fermi level, which could stabilize the countervailing native defects; for example, nitrogen vacancy (V_N) donors can compensate magnesium acceptors. As will be discussed in Sec. V, this is mitigated by the presence of passivating hydrogen impurities.

B. Donor dopants

Silicon substituting on the gallium site (Si_{Ga}),[46] oxygen substituting on the nitrogen site (O_N),[24,47] and germanium substituting on the gallium site (Ge_{Ga})[46,48,49] have all been identified to exhibit hydrogenic donor behavior and hence act as effective shallow donors in GaN. Although these donor impurities give rise to different breathing-mode relaxations of bonds with the nearest-neighbor atoms, all have small ionization energies and do not give rise to

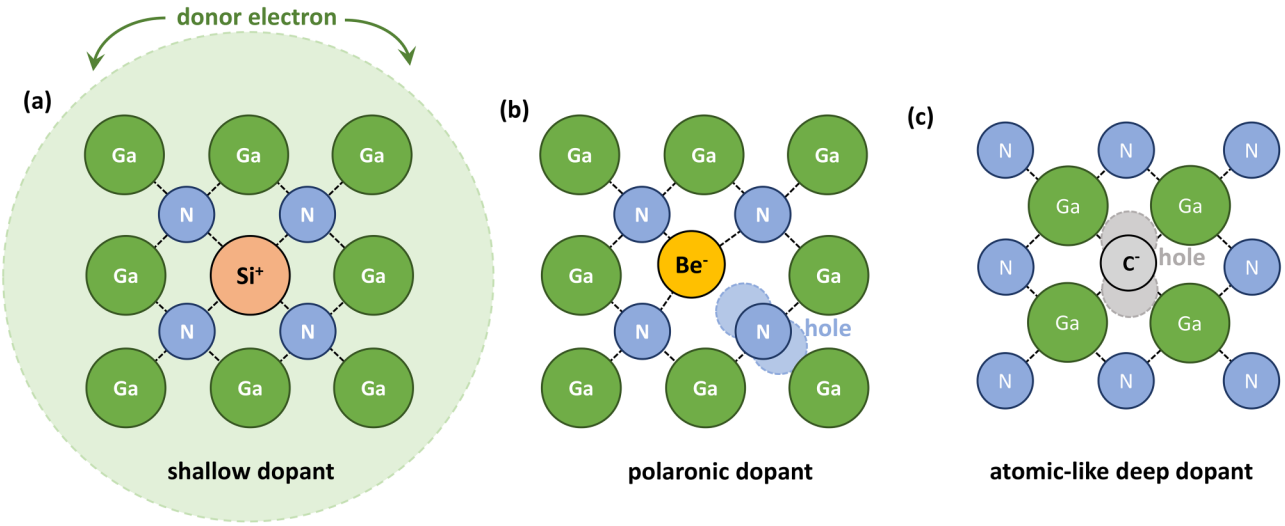

FIG. 1. Schematics of different types of dopant behavior in GaN, using specific examples, such as (a) Si_{Ga} as an effective-mass donor, (b) Be_{Ga} as a polaronic acceptor, and (c) C_N as an atomic-like defect. In each case, the dopant is in its neutral charge state, and electron/hole wavefunction behavior is illustrated with the lightly shaded shapes in each case.

deep defect levels. In some cases, germanium was demonstrated to be a more efficient dopant than silicon.[50–52] Sulfur and selenium, substituting on the nitrogen site, have also been found to be shallow donors in GaN and both may avoid the conductivity-limiting *DX* behavior (which will be further discussed in Sec. IX) in AlGaN alloys.[53]

Oxygen and silicon can also be background contaminants during growth,[54] which will be a concern when trying to achieve insulating material. In Sec. IV, we will discuss how deep acceptor dopants such as C can be added to compensate such unintentional *n*-type conductivity.

C. Acceptor dopants

Magnesium is the only acceptor known to be an effective *p*-type dopant in GaN. Substituting on the Ga site, Mg has been demonstrated to have an ionization near 200 meV.[55] This is close to the ionization energy estimated from effective-mass theory[56] (due to the heavy hole mass of the GaN valence band) but it means that *p*-type doping efficiencies are limited to only a few percent.

However, first-principles calculations have indicated that hole localization at next-nearest neighbors occurs even for the Mg_{Ga} acceptor.[57,58] As will be discussed in Sec. IV, such localization also occurs at other cation-site impurities,[59] leading them to exhibit high ionization energies and making them ineffective *p*-type dopants. Despite the localization predicted for Mg_{Ga} acceptors, their ionization energies are still small enough to lead to the presence of free holes. However, the presence of large concentrations of Mg^0_{Ga} may still have consequences for nitride devices, for instance, in causing internal optical loss in III-nitride optoelectronics.[60]

To overcome these limitations with candidate *p*-type dopants in GaN, alternative pathways to achieving *p*-type doping have been proposed. For example, *interstitial* fluorine F_i has been suggested to be a shallow acceptor in GaN and other wide-bandgap semiconductors, although this behavior has not been confirmed in experiments.[61] Polarization-induced hole conductivity has also been explored in GaN.[62]

IV. DEEP DOPANTS

In this section, we examine the properties of elements known to act as deep centers in GaN, including cation-site acceptors other than Mg_{Ga}. A few other impurities, acting as deep centers, have been intentionally added to GaN to alter its electrical or optical properties. Among these is C, which is incorporated into GaN to compensate *n*-type conductivity and yield semi-insulating behavior. Occasionally rare-earth (RE) impurities, such as Er and Eu, are also added to give rise to potentially useful optical transitions.

A. Cation-site acceptors

Impurities such as Zn, Cd, Be, and Ca have all been explored as alternative *p*-type dopants in GaN.[24,27,63–66] Like Mg_{Ga}, other cation-site acceptors in GaN trap holes onto a nearest-neighbor N atom [such as Be_{Ga}, which is depicted in Fig. 1(b)].[59] With a poor size match to the Ga cation, dopants such as Be, Ca, and Cd trap holes even more strongly than Mg, leading to higher ionization energies and even less effective doping behavior. Although Zn is a close size match to Mg, interactions between N 2*p* and Zn 3*d* orbitals lead to further stabilization of the Zn^0_{Ga} charge state, giving this acceptor a larger ionization energy (~450 meV) than Mg_{Ga}.[59,67] The success of Mg as an acceptor dopant can then be rationalized by its close size match to Ga, in addition to its lack of *d* orbitals.

Of course, other factors may limit the effectiveness of acceptor dopants in GaN. For instance, because of the small size of the Be atom, Be interstitials (Be_i) have moderate stability in GaN.[65,66,68] Similar behavior by Mg_i has also been explored in Mg doping.[69,70] The presence of these interstitial donors may thus lead to compensation. Another example is Zn_{Ga}, which can capture a second hole to become positively charged at low Fermi levels, further complicating *p*-type doping.[59]

Hole localization at polaronic acceptors leads to a characteristic local distortion, whereby the bond between the acceptor impurity and the nitrogen at which the hole is localized increases in length. This large distortion in the neutral charge states of these acceptors means that they exhibit large Stokes shifts in their optical transitions. Such deep, broad luminescence bands have been linked with the presence of these dopants in GaN.[27,59,71]

B. Carbon

Carbon is a common background impurity in GaN. However, C is also intentionally doped into GaN to create semi-insulating material.[72,73] Originally, this semi-insulating behavior was attributed to so-called "amphoteric" behavior of carbon; namely, that the introduction of carbon acceptors (C_N) and carbon donors (C_{Ga}) in nearly equal concentrations would establish a Fermi level near the middle of the bandgap.[74] However, achieving semi-insulating material with a specific Fermi level is notoriously difficult with such an approach. Such an explanation is no longer necessary, now that it has become clear that C_N is a deep acceptor,[36,75] which can by itself compensate any unintentional *n*-type dopants and pin the Fermi level deep in the bandgap, close to the deep acceptor level.

Substituting on the N site, carbon acts as an atomic-like acceptor in GaN with an ionization energy near 1 eV. The formation energy of C_N is shown in Fig. 2, plotted against the Fermi level which takes on values from 0 eV (the VBM) to 3.5 eV (the CBM). From such a diagram, the potential for a defect or impurity to incorporate can be determined by examining its formation energy (with smaller formation energies indicating a higher likelihood of incorporation), and how such stability depends on the position of the Fermi level.[16] Kinks in the plot (corresponding to equilibrium between two charge states) indicate a thermodynamic transition level of a given defect. When plotted for different conditions (such as Ga-poor or Ga-rich), such diagrams can also aid in determining how defect stability changes with growth conditions.

Deficient one electron relative to N, the acceptor hole of C_N is localized onto a C 2*p*-like orbital [as depicted in Fig. 1(c)]. These C-related states are still present when an electron is added to create C_N^-, making the behavior of these acceptors distinct from the polaronic cation-site acceptors. The deep acceptor behavior of C_N was recently confirmed via Hall effect experiments[73] and by capacitance transient spectroscopy.[76]

Despite nominally acting as an acceptor, C_N can also trap a second hole, becoming positively charged for Fermi levels near the

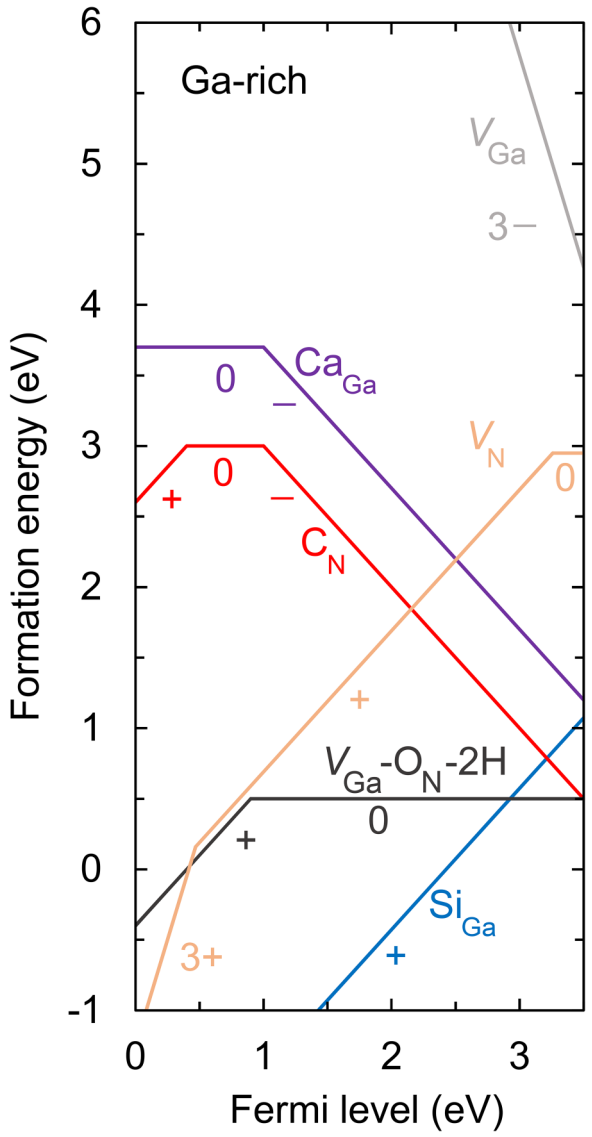

FIG. 2. Formation energy vs the Fermi level for a subset of native defects (V_{Ga} and V_N), impurities (C_N, Si_{Ga}, and Ca_{Ga}), and the V_{Ga}–O_N–2H complex in GaN under Ga-rich conditions. Diamond was used as a reference for C impurities, Si_3N_4 for Si, Ca_3N_2 for Ca, Ga_2O_3 for O, and H_2 for H. Labels of charge states are adjacent to each line segment. Data were adapted from Refs. 10, 36, 48, and 88.

VBM. This leads to the presence of a deep (+/0) donor transition level, predicted to be 0.4 eV above the VBM.[36] This second thermodynamic transition level was predicted to lead to a distinct optical transition,[36] which was subsequently confirmed in optical experiments.[77] This deep donor may also have implications in nitride devices as it could allow C_N to act as a hole trap.[78] This behavior has indeed been observed for C impurities in Mg-doped GaN.[79]

Depending on growth conditions and on the Fermi level position, carbon can also incorporate as a donor, for instance, as an interstitial (C_i) or on the Ga site (C_{Ga}).[36] C can also incorporate in a variety of complexes.[74,80,81] Optical and electronic experiments[82] suggest that incorporation in configurations other than C_N may be relevant only at high C concentrations.

C. Rare-earth impurities

Doping of GaN with RE elements has been suggested as a way of engineering sharp optical transitions that may be useful for solid-state lasers, optical fibers, light-emitting diodes, and other optoelectronic applications.[83,84] These transitions are thought to arise from the well-shielded *f* electrons of the RE elements. Early studies suggested that some RE elements, isoelectronic with Ga, do not introduce defect levels into the GaN bandgap.[85] However, by forming complexes with native defects, RE dopants may introduce deep levels into GaN.[86] More recent work has also suggested that Eu_{Ga} may introduce deep levels into GaN related both to polaronic localization [in the case of a deep (+/0) level] and due to highly localized 4*f* orbitals giving rise to atomic-like states [in the case of a deep (0/−) level].[87] For this reason, RE impurities may actually feature properties consistent with both Figs. 1(b) and 1(c).

V. UNINTENTIONAL IMPURITIES

Advances in the development of GaN devices have been due, in part, to the ability to achieve improved control over conductivity. Controlling the carrier concentration and carrier type in GaN has enabled *p*-type, *n*-type, and insulating material, which forms the basis for all electronic and optoelectronic devices. Achieving this control continues to pose a challenge; in particular, extrinsic sources such as the precursors used during growth, memory effects following prior growth, impurities introduced during substrate preparation steps, and the growth chamber itself can all act as sources of contamination. The type of impurity and the concentration that is incorporated depends, in part, on the type of growth method and environment that is used. This is summarized in Table I, where we list impurity concentrations identified using secondary ion mass spectrometry (SIMS) in GaN samples grown with different approaches.

TABLE I. Unintentional impurity concentrations (all in units of concentration 10^{16} cm^{-3}) measured by SIMS for GaN grown using different growth techniques as reported in the following references: hydride vapor-phase epitaxy (HVPE),[89,90] plasma-assisted molecular beam epitaxy (PAMBE),[91] metalorganic chemical vapor deposition (MOCVD),[90] and ammonothermal.[92] For each study, we list the highest reported value within the table below. Entries marked with x denote the impurity was not reported in the specific study.

Impurity	HVPE	PAMBE	MOCVD	Ammonothermal
H	26	60	24	20 000
O	2.3	9	2.2	2 000
Fe	0.33	x	x	20
C	23	2	13	10

A. Iron

As we have discussed in Sec. IV, one approach to mitigating the unintentional *n*-type conductivity and achieve (semi-)insulating material is to introduce compensating acceptors. One of the earlier demonstrations of this was work by Monemar and Lagerstedt,[93] whose GaN samples grown by hydride vapor-phase epitaxy were found to be insulating. Contamination by Fe and Cr unintentionally incorporated during growth was the source of this behavior. Fe is now widely used *intentionally* to achieve semi-insulating GaN buffer layers, a key requirement for high-frequency GaN devices.[94]

First-principles calculations have shown Fe is stable on the Ga site in GaN.[14] Substituting on the Ga site, Fe_{Ga} acts as an atomic-like deep acceptor [in analogy to Fig. 1(c)] with a (0/−) level (Fe^{3+}/Fe^{2+} if one uses the notation of the oxidation state of Fe) 3.0 eV above the GaN VBM, in agreement with photoluminescence excitation measurements[95] and deep-level transient spectroscopy measurements[96] of Fe-doped GaN. Hence, if Fe_{Ga} is the main impurity in GaN, this would lead to the Fermi level being pinned 0.5 eV below the CBM, producing semi-insulating material. In the neutral charge state, Fe^0_{Ga} is in a high-spin $S = 5/2$ configuration. This high-spin state leads to a sequence of excited states due to a combination of the tetrahedral crystal field and exchange splitting of the Fe 3*d* states. In the negative charge state, Fe^-_{Ga} is also stable in a high-spin $S = 2$ configuration, which in turn leads to a distinct sequence of excited states.[14]

The presence of Fe in GaN can also have a detrimental impact. Fe impurities in GaN have been linked to carrier trapping in III-nitride electronic devices[97,98] and have also been identified as an efficient SRH recombination center.[99] However, the microscopic mechanisms of Fe_{Ga} acting as an efficient SRH center remained elusive, given that the Fe_{Ga} (0/−) is very far from the GaN VBM and conventional wisdom would dictate that hole trapping is very slow, and that, therefore, Fe_{Ga} is an inefficient SRH center. This puzzle can be resolved by taking into account that the excited states of Fe_{Ga} can also participate in optical and nonradiative transitions. For example, the presence of Fe^0_{Ga} leads to sub-bandgap emission at 1.299 eV, which occurs due to transitions between the first excited state and the ground state of the Fe^0_{Ga} series.[95] First-principles calculations were instrumental in demonstrating that the excited states of Fe^0_{Ga} and Fe^-_{Ga} introduce new channels through which nonradiative recombination can occur, which in turn leads to a sizable hole capture coefficient and a large SRH recombination rate.[100]

The role of excited states of defects and their ability to lead to efficient recombination pathways has been highlighted for other defects in GaN,[12,13] underscoring the important role that first-principles calculations play in elucidating these phenomena.

B. Hydrogen

Hydrogen, a ubiquitous impurity in a range of growth and processing techniques, also strongly impacts the properties of GaN. Hydrogen is an amphoteric impurity in GaN, acting as a donor (H_i^+) in *p*-type material and as an acceptor (H_i^-) in *n*-type material, always counteracting the prevailing conductivity.[101] Positively charged H forms close bonds with a N anion, while negatively charged H incorporates at the octahedral interstitial site, where it is surrounded by Ga cations.

Hydrogen can also form complexes with native point defects and impurities. For example, gallium vacancies (V_{Ga}) can form complexes with H that have lower formation energies than bare V_{Ga}.[102] This is shown in Fig. 2, where the lower-energy V_{Ga}–O_N–2H complex (a gallium vacancy to which two hydrogen interstitials and one oxygen donor have bound) is plotted together with the higher-energy isolated V_{Ga}.

One might, therefore, think that the presence of hydrogen in GaN always leads to defect creation and that care should be taken to limit its incorporation. However, hydrogen can also be beneficial; indeed, it plays a key role in enabling *p*-type doping of GaN. When incorporated along with Mg [as happens in metalorganic chemical vapor deposition (MOCVD), the most widely used growth technique], H passivates the negatively charged acceptor, preventing a premature shift in the Fermi level that could lead to the incorporation of compensating V_N (see Fig. 2). A subsequent post-growth anneal breaks up the Mg−H complexes and activates the dopants, as was first experimentally demonstrated by Amano *et al.*[5] with electron beam irradiation and later by Nakamura *et al.*[103] who annealed Mg-doped GaN in a H-poor environment, leading to an increase in *p*-type conductivity. The microscopic origin of this phenomenon was later elucidated by first-principles calculations, which found that Mg−H complexes could dissociate at modest temperatures due to their low relatively low binding energy and the low diffusion barrier of H_i^+ in GaN.[101]

C. Calcium

Ca has recently been identified as an unintentional impurity incorporating via surface contamination (most likely introduced during wafer polishing) in molecular beam epitaxial (MBE) growth of GaN.[104] Calcium concentrations as high as 10^{18} cm^{-3} have been detected in MBE-grown quantum wells. Reductions in Ca concentrations were linked with a 10× increase in output power, suggesting that Ca impurities were a significant source of nonradiative recombination.

Using first-principles calculations, Shen *et al.* assessed the role of Ca in GaN.[10] They found that Ca prefers to substitute for Ga, where it acts as a deep acceptor. Trapping a highly localized hole in its neutral charge state, the behavior of Ca_{Ga} is analogous to Mg_{Ga}, and indicative of the polaronic acceptor behavior depicted in Fig. 1(b). However, Ca_{Ga} gives rise to a much higher ionization energy of 1 eV. In InGaN alloys, this (0/−) transition level approaches midgap, making Ca_{Ga} an efficient source of nonradiative recombination, and indicating that Ca impurities could severely limit the internal quantum efficiency of nitride-based LEDs.

VI. NATIVE DEFECTS

We have reviewed the properties of native defects in GaN in detail in Refs. 24 and 88. In general, native defects have formation energies significantly larger than those of impurities, as shown in Fig. 2. Among the most stable defects are V_N, which is most stable under *p*-type conditions, and V_{Ga}, which is most stable under *n*-type conditions. However, by forming complexes with impurities such as Mg, O, or H, these formation energies can be lowered, and the properties of the native defects can be modified.

A. Nitrogen vacancies

A vacancy in the nitrogen sublattice removes five valence electrons, leaving behind four gallium dangling bonds as depicted in Fig. 3(a). Removal of the remaining three valence electrons from these dangling bonds stabilizes positive charge states, and V_N can be stable from the 3+ to neutral charge state [with the (0/−) transition level occurring just above the CBM[88]], as shown in Fig. 2. Interaction between the electrons occupying these orbitals drives the behavior of V_N. When all electrons are removed, in the 3+ charge state, the nearest-neighbor Ga atoms move outward.

V_N is stable across most of the bandgap in the positive charge state, acting as a donor that might be expected to contribute to unintentional *n*-type conductivity (its formation energy is shown in Fig. 2). However, first-principles calculations have consistently indicated that the formation energy of V_N is high,[88,105–109] and that impurities (such as Si_{Ga} or O_N) are better candidates to explain the unintentional conductivity. Moreover, the (+/0) donor level of V_N is 0.2 eV below the CBM of GaN,[88,108] indicating that only a small fraction of donors would be ionized even if it were the dominant species.

However, the positively charged V_N can still form stable complexes with negatively charged impurities, behavior that was explored with early DFT calculations[69] and observed in positron annihilation spectroscopy (PAS) experiments.[110] Using hybrid functional calculations, Yan *et al.* found that negatively charged Mg_{Ga} formed favorable complexes with V_N[111] and could be a potential source of compensation and deep-level luminescence signals in Mg-doped GaN. In contrast, Miceli and Pasquarello have argued[70] that this complex may not be as relevant as other compensating species, such as Mg_i.

B. Gallium vacancies

The removal of a gallium atom takes away three valence electrons and leaves behind four nitrogen dangling bonds, as shown in Fig. 3(b). Upon filling or emptying these states, gallium vacancies in GaN can take charge states from 1+ to 3− and give rise to four thermodynamic transition levels in the bandgap.[88,108,109] Unlike for V_N, the dangling bond states of V_{Ga} do not strongly interact. Instead, as with the polaronic acceptor impurities, holes tend to localize onto these nearest-neighbor N 2*p* orbitals. When the Fermi level is near the CBM, they can be triply negatively charged but have high formation energies even under the most favorable conditions and are, thus, unlikely to incorporate as isolated species.[88,108,109] For instance, as shown in Fig. 2, isolated V_{Ga} is higher in energy than the C_N or Ca_{Ga} acceptor impurities under Ga-rich conditions. Although Ga-rich conditions do favor the incorporation of C_N over V_{Ga}, even under the N-rich extreme in *n*-type conditions, C_N^- is more than 1 eV more stable than V_{Ga}^{3-}.

However, by forming stable complexes with donor impurities, the formation energies of gallium vacancies can be considerably lowered. Since O and H are common contaminants during GaN growth that can be present as positively charged donors, they are natural candidates for forming complexes with V_{Ga}.[106] However, O replaces nearest-neighbor N atoms of the vacancy, H binds to the dangling bonds of these N atoms. Hybrid functional calculations have demonstrated that gallium vacancies can bind up to three of these impurities in stable complexes.[102] Subsequent studies have examined the role of donor-vacancy complexes in contributing to SRH recombination.[12,13]

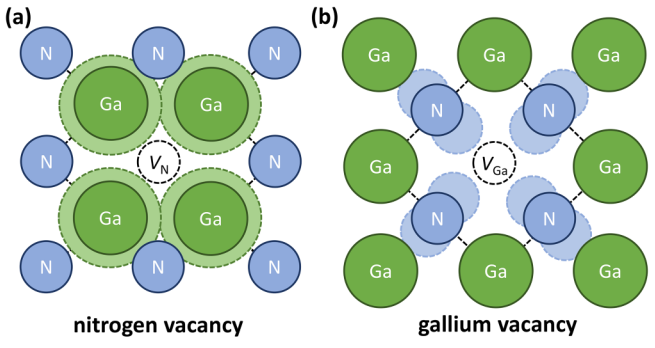

FIG. 3. Schematics of vacancy behavior in GaN for (a) V_N, whose behavior is derived mainly from interacting Ga 4*s* orbitals, and (b) V_{Ga}, whose behavior is driven by N dangling bonds comprised mainly of 2*p* orbitals.

C. Other native defects

Native interstitial and antisite defects have generally been found in previous studies to be high-energy defects.[24,88,108,109] Among these, gallium interstitials (Ga_i) have modest formation energies under *p*-type conditions but V_N are still lower in energy. Although these species have been detected at liquid helium temperatures after irradiation,[112] their low diffusion barrier means they will be highly mobile, even below room temperature, and are, thus, likely to move to the surface or annihilate.[107] Gallium antisite donors (Ga_N) also have their lowest energies under *p*-type conditions, but are still less stable than V_N, and unlikely to play a role in controlling the properties of GaN. Nitrogen interstitial (N_i) and antisite (N_{Ga}) defects are even higher in energy than Ga_N or Ga_i and, thus, even less likely to be relevant for the properties of GaN.

VII. IMPURITIES IN III-NITRIDE ALLOYS

Alloying GaN with Al enables direct bandgaps that can be tuned from 3.5 eV to 6.2 eV,[113] while alloying GaN with In enables direct bandgaps that can be tuned from ∼0.7 eV to 3.5 eV.[114] The direct bandgap of InGaN alloys has made optoelectronics spanning the visible range of the spectrum feasible.[1] Furthermore, the wide bandgap offered by AlGaN alloys enables power electronics and high-frequency devices where such large gaps are required. The ability to achieve controlled carrier concentrations is also desirable but remains a challenge in these alloys.

The ionization energy (ϵ_i) is a key property that determines the electronic and optical behavior of defects and impurities.[16] For devices comprised of III-nitride alloys, it is necessary to understand how ϵ_i changes as a function of the alloy content, i.e., as the band edges shift with composition. We can align the band edges of the III-nitrides on an absolute scale, as illustrated in Fig. 4. Note that the valence-band offsets are much smaller than the conduction-band offsets.[44] Performing first-principles calculations for random

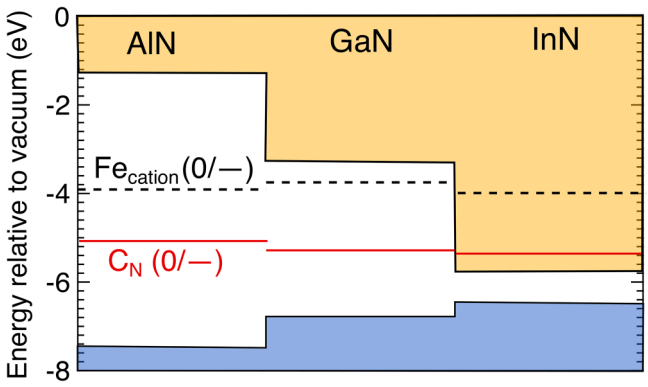

FIG. 4. Charge state transition levels of the (0/−) acceptor levels of C_N (red solid line)[36] and Fe_{cation} (black dotted line)[14] in AlN, GaN, and InN with the valence and conduction bands aligned[24] on an absolute energy scale.

alloys is very difficult. For InGaN alloys, we demonstrated that the main effect of alloying on the bandgap, band edges, and defect levels is due to the change in lattice parameters. Results for *deep* defects and impurities can then be obtained by performing standard supercell calculations using a GaN supercell with lattice parameters modified to match the InGaN lattice parameters based on Vegard's law.[10,13,23]

Several important insights can be obtained from these calculations. First, defect levels that are derived from N states follow the InGaN VBM as a function of indium content, while defects that are comprised of cation states track the conduction band. Atomic impurities, where the defect level is composed of the impurity state, lead to thermodynamic transition levels that remain constant on an absolute scale as a function of alloy content. We also expect the same qualitative considerations that connect the atomic states of defect levels with the host material band edges to apply in the case of AlGaN alloys. This is confirmed by first-principles calculations showing that the thermodynamic transition levels of atomic-like impurities such as C_N[36] and Fe on the cation site Fe_{cation}[14] align on an absolute scale across GaN, InN, and AlN, as illustrated in Fig. 4. This can be understood based on the fact that the C_N (0/−) level is derived from C 2*p* states and the Fe_{cation} (0/−) level is derived from Fe 3*d* states in each of the III-nitrides.

For the case of *shallow* donors and acceptors in GaN, it is important to understand whether they will continue to be effective dopants in alloys with In and Al. For the shallow donors (Si, Ge, and O) and shallow acceptor (Mg) in GaN, it has been shown that these impurities continue to behave as shallow defects in InN.[115] Hence, we would expect that these impurities, if present in InGaN alloys, will contribute to conductivity. Achieving such conductivity is more challenging in AlN, as will be discussed in Sec. IX.

VIII. EXPERIMENTAL SIGNATURES OF DEEP IMPURITIES

The ability to control and manipulate point defects in semiconductors is predicated upon identifying their chemical identity, their electrical behavior, and the position of defect levels within the bandgap in the case of deep defects. A range of experimental techniques have been applied to identify and elucidate the properties of defects in GaN, including SIMS,[116] PAS,[110,117,118] x-ray measurements,[119] electron paramagnetic resonance,[95,120] capacitive junction spectroscopy,[76,96,121] deep-level transient spectroscopy (DLTS),[122,123] deep-level optical spectroscopy (DLOS),[122] vibrational spectroscopy,[31,124] and photoluminescence (PL) spectroscopy.[125] Each of these techniques yields either the electronic, vibrational, optical, structural, or chemical identity of a defect within the lattice. Interpreting these experimental signals has been complemented by advances in first-principles calculations which have enabled the accurate description of defect properties.[16]

In some of these techniques, such as PL spectroscopy, DLTS, or DLOS, the measured signal is a signature of how the atomic and electronic structures of the defect are coupled. A powerful approach for analyzing and interpreting these interactions is to invoke the Franck–Condon principle and construct a configuration coordinate diagram (as explained by Alkauskas *et al.* in the Tutorial of Ref. 25). However, one needs to exercise care in comparing DFT results for ionization energies with experimental quantities.

For example, an optical absorption or emission process involving a deep defect may lead to large lattice relaxation which would result in the peak absorption and emission energies that differ from the ionization energy of the defect. This can be described using a configuration coordinate diagram and is shown for the case of the Fe_{Ga} impurity in GaN in Fig. 5. It is clear that there is a large energy difference between the peak absorption and emission energies (denoted by vertical arrows in Fig. 5) and the ionization energy of Fe_{Ga}. In Fig. 6, we summarize the peak emission energies for some impurities in GaN that are also known to exhibit large differences between their peak emission energy and ionization energy.

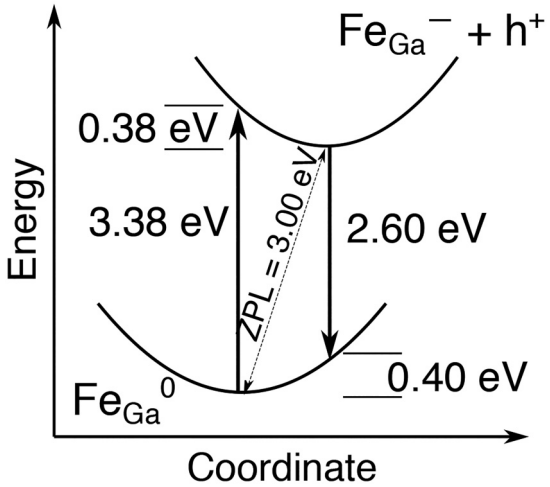

FIG. 5. Configuration coordinate diagram for Fe_{Ga} illustrating optical transitions that involve the valence band and the Fe_{Ga} (0/−) level. Details on how to interpret configuration coordinate diagrams can be found in Ref. 25.

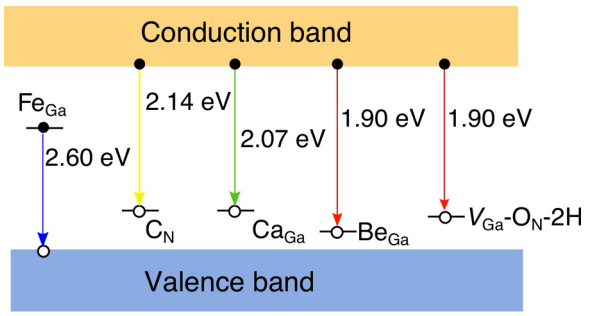

FIG. 6. Peak emission energies involving Fe_{Ga}, C_N, Ca_{Ga}, Be_{Ga} impurities and impurity complexes with V_{Ga} as reported in Refs. 10, 14, 36, and 59.

In a DLTS measurement, the transient change in the depletion capacitance of a Schottky or *pn* junction is measured as charge carriers are thermally emitted from deep defect levels to the band edge. To interpret this measurement, one applies the principle of detailed balance to relate the thermal emission rate with the rate of the carrier capture process.[126] Since DLTS measurements rely on thermal emission to determine the activation energy of defects, they are sensitive to defects that are within ~1 eV of a band edge. To probe defects that are deeper within the bandgap, DLOS measurements can be performed, where the thermal emission of charge carriers trapped at defects is replaced with sub-bandgap photoexcitation. Photoionization of the trapped charges leads to a change in the depletion capacitance as a function of the excitation wavelength. These changes in capacitance are fit to empirical models for photoionization cross sections[121] to determine the position of the defect levels within the bandgap.

DLTS and DLOS measurements in conjunction with first-principles calculations can, thus, be used to identify the microscopic origin of defects in wide-bandgap semiconductors such as GaN. However, one must exercise caution when comparing DLTS or DLOS results with first-principles calculations of defect ionization energies. For example, since DLTS measurements are conducted under conditions where the temperature is varied, it is important to properly account for the temperature dependence of all quantities. This requires going beyond the $T = 0$ K static-lattice DFT calculations and considering the effects of finite temperature, including renormalization of the band structure of the semiconductor due to electron–phonon and thermal expansion effects, the change in the defect level due to vibrational entropy,[127] and the temperature dependence of the nonradiative carrier capture and thermal emission rates.[20] Indeed, first-principles calculations have shown that if these finite-temperature effects are accounted for, defects in GaN that have similar ionization energies can have very different activation energies in DLTS due to these temperature-dependent effects.[21]

IX. OUTLOOK ON DEFECTS AND DOPING IN NITRIDE SEMICONDUCTORS BEYOND GaN

There are a number of other nitride semiconductors beyond GaN that are being explored for applications in electronic and optoelectronic devices, including aluminum nitride,[113] the hexagonal and cubic polymorphs of boron nitride,[128,129] the II–IV-nitrides,[130,131] and the transition metal nitrides such as ScN and TiN.[132,133] Below, we discuss how the insights gained from GaN might be applied in these systems and articulate some of the research opportunities associated with these novel semiconductors.

A. AlN

Like GaN, AlN is stable in the wurtzite structure but it has a much wider bandgap along with a lower-lying valence band and a higher-lying conduction band (see Fig. 4).[24] As a result, many of the issues that are detrimental to dopant effectiveness in GaN are exacerbated in AlN. Magnesium acceptors are also afflicted by hole localization in AlN and have even larger ionization energies than in GaN.[58,134,135] Other cation-site acceptor dopants also exhibit hole trapping with larger ionization energies than in GaN.[45,135]

Donor doping is also more problematic in AlN than in GaN. A major difference with GaN is the presence of *DX* behavior, whereby a positively charged donor captures two electrons, becoming negatively charged and leading to self-compensation. This behavior occurs for silicon, oxygen, and germanium donors in AlN.[48] Among these, Si_{Al} is the most effective donor; despite being a *DX* center its (+/−) transition level is only 150 meV from the CBM of AlN. These levels occur much deeper in the gap for O_N (0.64 eV) and Ge_{Al} (1.05 eV), making them ineffective donors.

As in GaN, the most relevant native defects in AlN are the vacancies.[136–138] Like V_{Ga}, V_{Al} is a hole-trapping acceptor that can form complexes with donor impurities. Near the CBM, V_{Al}^{3-} has a formation energy near zero under Al-rich conditions, suggesting it is an important compensating defect in *n*-type AlN. V_N in AlN has a low formation energy under *p*-type conditions.

B. BN

Boron nitride is an ultra-wide-bandgap nitride semiconductor that is stable in the hexagonal, cubic, and wurtzite polymorphs.[128] Hexagonal boron nitride (*h*-BN) is a wide-bandgap insulator with an indirect bandgap of 6.08 eV.[129] The layered crystal structure has led to it being used extensively in the field of two-dimensional materials.[139] The wide bandgap of BN also makes it a promising candidate as a channel material for power electronic devices due to the potential to achieve large breakdown fields.[113] However, epitaxial growth of this material remains challenging.

Preliminary experimental studies of Si doping in *c*-BN have demonstrated electron concentrations that exceed 10^{17} cm^{-3}.[140] Experiments[141–143] have indicated that Be doping of c-BN could lead to *p*-type conductivity with an activation energy near 0.2 eV. This was confirmed by first-principles calculations that found Be is a shallow acceptor in *c*-BN with an ionization energy of 0.24 eV close to that of Mg in GaN.[144] The prospect of achieving controlled ambipolar doping in *c*-BN, combined with its wide-bandgap (>6 eV),[145] and ultra-high thermal conductivity[146] make *c*-BN a compelling candidate for power electronics. In contrast, first-principles studies have shown candidate *n*- and *p*-type dopants in *h*-BN are all deep[144,147] and are unlikely to lead to controlled doping.

C. Transition metal nitrides

The transition metal nitrides ScN and YN are semiconductors that are stable in the rock salt phase. The identification of large piezoelectric and ferroelectric polarization in ScAlN alloys[148] and the low lattice mismatch between GaN and ScN[149] have prompted investigations into achieving polarization engineering at GaN/ScN interfaces. Recent first-principles calculations have suggested it is possible to achieve large bound charges at the interface between ScN and GaN.[133] Controlling the conductivity in the transition metal nitrides will be essential for enabling such applications. ScN is a low-bandgap semiconductor with a bandgap of ∼0.9 eV[150,151] and a conduction band that is low on an absolute scale, similar to InN.[151] This would suggest that as-grown ScN is prone to be *n*-type, consistent with results of hybrid functional calculations for defects and impurities in ScN.[151] Mg acceptors were found to be shallow acceptors in ScN,[151] and, thus, bipolar doping is apparently possible in this material.

D. II–IV-nitrides

The ternary nitrides, including Zn–IV-nitrides such as $ZnGeN_2$, $ZnSnN_2$, and $ZnSiN_2$ are another class of nitride materials. Studied since the 1970s,[152] these materials offer added flexibility in lattice and bandgap engineering of nitride alloys. These systems are based on the wurtzite III-nitrides, but in which a pair of group-III cations is replaced by one Zn atom and one group-IV element (either Si, Ge, or Sn), transforming the structure from wurtzite to orthorhombic. Such materials obey the octet criteria for bonding, and the choice in group-IV element determines the lattice constant and the bandgap of the compound.[153]

The presence of two different cations in the orthorhombic structure of the II–IV-nitrides leads to the additional possibility of cation antisite defects (e.g., Zn_{Ge} and Ge_{Zn} in the case of $ZnGeN_2$). Such defects and their complexes have been found to be quite stable and may in fact play a role in determining charge neutrality.[154,155] The presence of the two different cations also makes *p*-type doping in these materials challenging due to the potential for substitution on the wrong site. For example, in $ZnGeN_2$, Al_{Ge} is an acceptor with a low ionization energy while Al_{Zn} is a donor. This could lead to self-compensation. To counteract this, co-doping with hydrogen (similar to its use in *p*-type doping of GaN with Mg) has been proposed as a means to achieve *p*-type doping in $ZnGeN_2$.[156] *n*-type doping is expected to be straightforward; e.g., group-V elements substituting on the Ge site, and group-VI elements on the nitrogen site act as shallow donors in $ZnGeN_2$.[155]

X. CONCLUSIONS

In this Tutorial, we have described the basic principles of dopants, defects, and impurities in GaN from a theoretical perspective. Many donor dopants exhibit effective-mass behavior in GaN, whereas most acceptor dopants exhibit deep behavior and large ionization energies. Native defects are generally high in energy, though by forming complexes with impurities their formation energy can be lowered. Polaronic hole trapping affects many acceptors, while other impurities (such as Fe and C) have atomic-like deep defect behavior. With knowledge of band offsets, the properties of these defects and impurities can also be predicted in III-nitride alloys, and recent explicit alloy calculations have confirmed these predictions. These principles can be extrapolated to provide insights into the behavior of other novel wide-bandgap semiconductors such as aluminum nitride and boron nitride.

ACKNOWLEDGMENTS

J.L.L. and D.W. were supported by the Office of Naval Research through the Naval Research Laboratory's Basic Research Program. C.G.V.d.W was supported by the U.S. Department of Energy (DOE), Office of Science, Basic Energy Sciences (BES) under Award No. DE-SC0010689. Computations were performed at the DoD Supercomputing Resource Center at ARL, and at the National Energy Research Scientific Computing Center (NERSC), a U.S. Department of Energy Office of Science User Facility operated under Contract No. DE-AC02-05CH11231.

DATA AVAILABILITY

Data sharing is not applicable to this article as no new data were created or analyzed in this study.

REFERENCES

[1]S. Pimputkar, J. S. Speck, S. P. DenBaars, and S. Nakamura, Nat. Photonics **3**, 180 (2009).
[2]M. T. Hardy, D. F. Feezell, S. P. DenBaars, and S. Nakamura, Mater. Today **14**, 408 (2011).
[3]U. K. Mishra, L. Shen, T. E. Kazior, and Y. Wu, Proc. IEEE **96**, 287 (2008).
[4]A. Goyal, P. Gorai, S. Anand, E. S. Toberer, G. J. Snyder, and V. Stevanović, Chem. Mater. **32**, 4467 (2020).
[5]H. Amano, M. Kito, K. Hiramatsu, and I. Akasaki, Jpn. J. Appl. Phys. **28**, L2112 (1989).
[6]S. Nakamura, T. Mukai, M. Senoh, and N. Iwasa, Jpn. J. Appl. Phys. **31**, L139 (1992).
[7]T. J. Anderson, B. N. Feigelson, F. J. Kub, M. J. Tadjer, K. D. Hobart, M. A. Mastro, J. K. Hite, and C. R. Eddy, Electron. Lett. **50**, 197 (2014).
[8]T. Narita, K. Tomita, K. Kataoka, Y. Tokuda, T. Kogiso, H. Yoshida, N. Ikarashi, K. Iwata, M. Nagao, N. Sawada, M. Horita, J. Suda, and T. Kachi, Jpn. J. Appl. Phys. **59**, SA0804 (2019).
[9]R. Collazo, J. Xie, B. E. Gaddy, Z. Bryan, R. Kirste, M. Hoffmann, R. Dalmau, B. Moody, Y. Kumagai, T. Nagashima, Y. Kubota, T. Kinoshita, A. Koukitu, D. L. Irving, and Z. Sitar, Appl. Phys. Lett. **100**, 191914 (2012).
[10]J.-X. Shen, D. Wickramaratne, C. E. Dreyer, A. Alkauskas, E. Young, J. S. Speck, and C. G. Van de Walle, Appl. Phys. Expr. **10**, 021001 (2017).
[11]L. Shi and L.-W. Wang, Phys. Rev. Lett. **109**, 245501 (2012).
[12]A. Alkauskas, C. E. Dreyer, J. L. Lyons, and C. G. Van de Walle, Phys. Rev. B **93**, 201304 (2016).
[13]C. E. Dreyer, A. Alkauskas, J. L. Lyons, J. S. Speck, and C. G. Van de Walle, Appl. Phys. Lett. **108**, 141101 (2016).
[14]D. Wickramaratne, J.-X. Shen, C. E. Dreyer, A. Alkauskas, and C. G. Van de Walle, Phys. Rev. B **99**, 205202 (2019).
[15]A. M. Stoneham, *Theory of Defects in Solids: Electronic Structure of Defects in Insulators and Semiconductors* (Oxford University Press, 2001).
[16]C. Freysoldt, B. Grabowski, T. Hickel, J. Neugebauer, G. Kresse, A. Janotti, and C. G. Van de Walle, Rev. Mod. Phys. **86**, 253 (2014).
[17]A. Alkauskas, J. L. Lyons, D. Steiauf, and C. G. Van de Walle, Phys. Rev. Lett. **109**, 267401 (2012).
[18]Y. K. Frodason, K. M. Johansen, L. Vines, and J. B. Varley, J. Appl. Phys. **127**, 075701 (2020).

[19]C. E. Dreyer, A. Alkauskas, J. L. Lyons, and C. G. Van de Walle, Phys. Rev. B **102**, 085305 (2020).
[20]A. Alkauskas, Q. Yan, and C. G. Van de Walle, Phys. Rev. B **90**, 075202 (2014).
[21]D. Wickramaratne, C. E. Dreyer, B. Monserrat, J.-X. Shen, J. L. Lyons, A. Alkauskas, and C. G. Van de Walle, Appl. Phys. Lett. **113**, 192106 (2018).
[22]J. S. Harris, B. E. Gaddy, R. Collazo, Z. Sitar, and D. L. Irving, Phys. Rev. Mater. **3**, 054604 (2019).
[23]D. Wickramaratne, C. E. Dreyer, J.-X. Shen, J. L. Lyons, A. Alkauskas, and C. G. Van de Walle, Phys. Status Solidi B **257**, 1900534 (2020).
[24]C. G. Van de Walle and J. Neugebauer, J. Appl. Phys. **95**, 3851 (2004).
[25]A. Alkauskas, M. D. McCluskey, and C. G. Van de Walle, J. Appl. Phys. **119**, 181101 (2016).
[26]S. J. Pearton, J. C. Zolper, R. J. Shul, and F. Ren, J. Appl. Phys. **86**, 1 (1999).
[27]M. A. Reshchikov and H. Morkoç, J. Appl. Phys. **97**, 061301 (2005).
[28]C. R. Eddy, J. K. Hite, N. Nepal, and M. A. Mastro, J. Vac. Sci. Technol. A **31**, 05851 (2013).
[29]P. Pampili and P. J. Parbrook, Mater. Sci. Semicond. Process. **62**, 180 (2017).
[30]R. A. Ferreyra, C. Zhu, A. Teke, and H. Morkoç, "Group-III nitrides," in *Springer Handbook of Electronic and Photonic Materials*, edited by S. Kasap and P. Capper (Springer International Publishing, 2017), pp. 1–1.
[31]M. Stavola and W. B. Fowler, J. Appl. Phys. **123**, 161561 (2018).
[32]H.-P. Komsa, T. T. Rantala, and A. Pasquarello, Phys. Rev. B **86**, 045112 (2012).
[33]S. Lany and A. Zunger, Phys. Rev. B **78**, 235104 (2008).
[34]C. Freysoldt, J. Neugebauer, and C. G. Van de Walle, Phys. Rev. Lett. **102**, 016402 (2009).
[35]C. Freysoldt, J. Neugebauer, and C. G. Van de Walle, Phys. Status Solidi B **248**, 1067 (2011).
[36]J. L. Lyons, A. Janotti, and C. G. Van de Walle, Phys. Rev. B **89**, 035204 (2014).
[37]S. C. Erwin, L. Zu, M. I. Haftel, A. L. Efros, T. A. Kennedy, and D. J. Norris, Nature **436**, 91 (2005).
[38]M. Wang, S. Mu, and C. G. Van de Walle, ACS Appl. Mat. Interfaces **13**(8), 10650–10655 (2021).
[39]A. J. Ptak, L. J. Holbert, L. Ting, C. H. Swartz, M. Moldovan, N. C. Giles, T. H. Myers, P. Van Lierde, C. Tian, R. A. Hockett, S. Mitha, A. E. Wickenden, D. D. Koleske, and R. L. Henry, Appl. Phys. Lett. **79**, 2740 (2001).
[40]S. C. Cruz, S. Keller, T. E. Mates, U. K. Mishra, and S. P. DenBaars, J. Cryst. Growth **311**, 3817 (2009).
[41]T. K. Zywietz, J. Neugebauer, and M. Scheffler, Appl. Phys. Lett. **74**, 1695 (1999).
[42]P. Kempisty, Y. Kangawa, A. Kusaba, K. Shiraishi, S. Krukowski, M. Bockowski, K. Kakimoto, and H. Amano, Appl. Phys. Lett. **111**, 141602 (2017).
[43]W. Kohn and J. M. Luttinger, Phys. Rev. **98**, 915 (1955).
[44]C. G. Van de Walle and J. Neugebauer, Nature **423**, 626 (2003).
[45]J. L. Lyons, A. Janotti, and C. G. Van de Walle, J. Appl. Phys. **115**, 012014 (2014).
[46]P. Bogusławski and J. Bernholc, Phys. Rev. B **56**, 9496 (1997).
[47]T. Mattila and R. M. Nieminen, Phys. Rev. B **54**, 16676 (1996).
[48]L. Gordon, J. L. Lyons, A. Janotti, and C. G. Van de Walle, Phys. Rev. B **89**, 085204 (2014).
[49]C. Nenstiel, G. Callsen, F. Nippert, T. Kure, S. Schlichting, N. Jankowski, M. P. Hoffmann, A. Dadgar, S. Fritze, A. Krost, M. R. Wagner, A. Hoffmann, and F. Bechstedt, Commun. Phys. **1**, 38 (2018).
[50]C. Nenstiel, M. Bügler, G. Callsen, F. Nippert, T. Kure, S. Fritze, A. Dadgar, H. Witte, J. Bläsing, A. Krost, and A. Hoffmann, Phys. Status Solidi RRL **9**, 716 (2015).
[51]M. Iwinska, N. Takekawa, V. Ivanov, M. Amilusik, P. Kruszewski, R. Piotrzkowski, E. Litwin-Staszewska, B. Lucznik, M. Fijalkowski, T. Sochacki, H. Teisseyre, H. Murakami, and M. Bockowski, J. Cryst. Growth **480**, 102 (2017).
[52]J. N. Baker, P. C. Bowes, J. S. Harris, R. Collazo, Z. Sitar, and D. L. Irving, Appl. Phys. Lett. **117**, 102109 (2020).
[53]L. Gordon, J. B. Varley, J. L. Lyons, A. Janotti, and C. G. Van de Walle, Phys. Status Solidi RRL **9**, 462 (2015).
[54]G. Pozina, S. Khromov, C. Hemmingsson, L. Hultman, and B. Monemar, Phys. Rev. B **84**, 165213 (2011).
[55]W. Götz, N. M. Johnson, J. Walker, D. P. Bour, and R. A. Street, Appl. Phys. Lett. **68**, 667 (1996).
[56]S. Fischer, C. Wetzel, E. E. Haller, and B. K. Meyer, Appl. Phys. Lett. **67**, 1298 (1995).
[57]S. Lany and A. Zunger, Appl. Phys. Lett. **96**, 142114 (2010).
[58]J. L. Lyons, A. Janotti, and C. G. Van de Walle, Phys. Rev. Lett. **108**, 156403 (2012).
[59]J. L. Lyons, A. Janotti, and C. G. Van de Walle, Jpn. J. Appl. Phys. **52**, 08JJ04 (2013).
[60]E. Kioupakis, P. Rinke, and C. G. Van de Walle, Appl. Phys. Expr. **3**, 082101 (2010).
[61]A. Janotti, E. Snow, and C. G. Van de Walle, Appl. Phys. Lett. **95**, 172109 (2009).
[62]R. Chaudhuri, S. J. Bader, Z. Chen, D. A. Muller, H. G. Xing, and D. Jena, Science **365**, 1454 (2019).
[63]S. Nakamura, J. Cryst. Growth **145**, 911 (1994).
[64]F. Bernardini, V. Fiorentini, and A. Bosin, Appl. Phys. Lett. **70**, 2990 (1997).
[65]C. G. Van de Walle, S. Limpijumnong, and J. Neugebauer, Phys. Rev. B **63**, 245202 (2001).
[66]H. T. Wang, L. S. Tan, and E. F. Chor, J. Cryst. Growth **268**, 489 (2004).
[67]S. Strite, Jpn. J. Appl. Phys. **33**, L699 (1994).
[68]F. Tuomisto, V. Prozheeva, I. Makkonen, T. H. Myers, M. Bockowski, and H. Teisseyre, Phys. Rev. Lett. **119**, 196404 (2017).
[69]F. A. Reboredo and S. T. Pantelides, Phys. Rev. Lett. **82**, 1887 (1999).
[70]G. Miceli and A. Pasquarello, Phys. Rev. B **93**, 165207 (2016).
[71]M. Ilegems and R. Dingle, J. Appl. Phys. **44**, 4234 (1973).
[72]S. W. Kaun, M. Hoi Wong, J. Lu, U. K. Mishra, and J. S. Speck, Electron. Lett. **49**, 893 (2013).
[73]M. Iwinska, R. Piotrzkowski, E. Litwin-Staszewska, T. Sochacki, M. Amilusik, M. Fijalkowski, B. Lucznik, and M. Bockowski, Appl. Phys. Expr. **10**, 011003 (2016).
[74]A. F. Wright, J. Appl. Phys. **92**, 2575 (2002).
[75]J. L. Lyons, A. Janotti, and C. G. Van de Walle, Appl. Phys. Lett. **97**, 152108 (2010).
[76]K. Kanegae, T. Narita, K. Tomita, T. Kachi, M. Horita, T. Kimoto, and J. Suda, Jpn. J. Appl. Phys. **59**, SGGD05 (2020).
[77]M. A. Reshchikov, M. Vorobiov, D. O. Demchenko, U. Özgür, H. Morkoç, A. Lesnik, M. P. Hoffmann, F. Hörich, A. Dadgar, and A. Strittmatter, Phys. Rev. B **98**, 125207 (2018).
[78]J. L. Lyons, K. Krishnaswamy, L. Gordon, A. Janotti, and C. G. Van de Walle, IEEE Electron Device Lett. **37**, 154 (2016).
[79]T. Narita, K. Tomita, Y. Tokuda, T. Kogiso, M. Horita, and T. Kachi, J. Appl. Phys. **124**, 215701 (2018).
[80]D. O. Demchenko, I. C. Diallo, and M. A. Reshchikov, J. Appl. Phys. **119**, 035702 (2016).
[81]M. Matsubara and E. Bellotti, J. Appl. Phys. **121**, 195701 (2017).
[82]M. E. Zvanut, S. Paudel, E. R. Glaser, M. Iwinska, T. Sochacki, and M. Bockowski, J. Electron. Mater. **48**, 2226 (2019).
[83]A. Steckl and J. Zavada, MRS Bull. **24**, 33 (1999).
[84]B. Mitchell, V. Dierolf, T. Gregorkiewicz, and Y. Fujiwara, J. Appl. Phys. **123**, 160901 (2018).
[85]J.-S. Filhol, R. Jones, M. J. Shaw, and P. R. Briddon, Appl. Phys. Lett. **84**, 2841 (2004).
[86]K. Hoang, Phys. Status Solidi RRL **10**, 915 (2016).
[87]K. Hoang, Phys. Rev. Mater. **5**, 034601 (2021).
[88]J. L. Lyons and C. G. Van de Walle, npj Comput. Mater. **3**, 12 (2017).

[89]F. Zimmermann, F. Beyer, G. Gärtner, C. Röder, N. Son, E. Janzén, D. Veselá, J. Lorinčík, P. Hofmann, M. Krupinski, T. Mikolajick, F. Habel, G. Leibiger, and J. Heitmann, Opt. Mater. **70**, 127 (2017).
[90]J. Meyer, R. Liu, R. Schaller, H.-P. Lee, and C. Bayram, J. Phys. Photonics **2**, 035003 (2020).
[91]B. M. McSkimming, C. Chaix, and J. S. Speck, J. Vac. Sci. Technol. A **33**, 05E128 (2015).
[92]S. Pimputkar, S. Kawabata, J. S. Speck, and S. Nakamura, J. Cryst. Growth **403**, 7 (2014).
[93]B. Monemar and O. Lagerstedt, J. Appl. Phys. **50**, 6480 (1979).
[94]J. Freitas, Jr., M. Gowda, J. Tischler, J.-H. Kim, L. Liu, and D. Hanser, J. Cryst. Growth **310**, 3968 (2008).
[95]E. Malguth, A. Hoffmann, W. Gehlhoff, O. Gelhausen, M. Phillips, and X. Xu, Phys. Rev. B **74**, 165202 (2006).
[96]A. Polyakov, N. Smirnov, A. Govorkov, N. Pashkova, A. Shlensky, S. Pearton, M. Overberg, C. Abernathy, J. Zavada, and R. Wilson, J. Appl. Phys. **93**, 5388 (2003).
[97]M. Silvestri, M. J. Uren, and M. Kuball, Appl. Phys. Lett. **102**, 073501 (2013).
[98]W. Sun, J. L. Jimenez, and A. R. Arehart, IEEE Electron Device Lett. **41**, 816 (2020).
[99]T. Uždavinys, S. Marcinkevičius, J. Leach, K. Evans, and D. C. Look, J. Appl. Phys. **119**, 215706 (2016).
[100]D. Wickramaratne, J.-X. Shen, C. E. Dreyer, M. Engel, M. Marsman, G. Kresse, S. Marcinkevičius, A. Alkauskas, and C. G. Van de Walle, Appl. Phys. Lett. **109**, 162107 (2016).
[101]J. Neugebauer and C. G. Van de Walle, Phys. Rev. Lett. **75**, 4452 (1995).
[102]J. L. Lyons, A. Alkauskas, A. Janotti, and C. G. Van de Walle, Phys. Status Solidi B **252**, 900 (2015).
[103]S. Nakamura, N. Iwasa, M. Senoh, and T. Mukai, Jap. J. Appl. Phys. **31**, 1258 (1992).
[104]E. C. Young, N. Grandjean, T. E. Mates, and J. S. Speck, Appl. Phys. Lett. **109**, 212103 (2016).
[105]C. G. Van de Walle and J. Neugebauer, Phys. Rev. B **50**, 8067 (1994).
[106]T. Mattila and R. M. Nieminen, Phys. Rev. B **55**, 9571 (1997).
[107]S. Limpijumnong and C. G. Van de Walle, Phys. Rev. B **69**, 035207 (2004).
[108]G. Miceli and A. Pasquarello, Microelectron. Eng. **147**, 51 (2015).
[109]I. C. Diallo and D. O. Demchenko, Phys. Rev. Appl. **6**, 064002 (2016).
[110]S. Hautakangas, J. Oila, M. Alatalo, K. Saarinen, L. Liszkay, D. Seghier, and H. P. Gislason, Phys. Rev. Lett. **90**, 137402 (2003).
[111]Q. Yan, A. Janotti, M. Scheffler, and C. G. Van de Walle, Appl. Phys. Lett. **100**, 142110 (2012).
[112]K. H. Chow, G. D. Watkins, A. Usui, and M. Mizuta, Phys. Rev. Lett. **85**, 2761 (2000).
[113]J. Y. Tsao, S. Chowdhury, M. A. Hollis, D. Jena, N. M. Johnson, K. A. Jones, R. J. Kaplar, S. Rajan, C. G. Van de Walle, E. Bellotti, C. L. Chua, R. Collazo, M. E. Coltrin, J. A. Cooper, K. R. Evans, S. Graham, T. A. Grotjohn, E. R. Heller, M. Higashiwaki, M. S. Islam, P. W. Juodawlkis, M. A. Khan, A. D. Koehler, J. H. Leach, U. K. Mishra, R. J. Nemanich, R. C. N. Pilawa-Podgurski, J. B. Shealy, Z. Sitar, M. J. Tadjer, A. F. Witulski, M. Wraback, and J. A. Simmons, Adv. Electron. Mater. **4**, 1600501 (2018).
[114]V. Davydov, A. Klochikhin, V. Emtsev, D. Kurdyukov, S. Ivanov, V. Vekshin, F. Bechstedt, J. Furthmüller, J. Aderhold, J. Graul, A. Mudryi, H. Harima, A. Hashimoto, A. Yamamoto, and E. Haller, Phys. Status Solidi B **234**, 787 (2002).
[115]C. G. Van de Walle, J. L. Lyons, and A. Janotti, Phys. Status Solidi A **207**, 1024 (2010).
[116]D. Meister, M. Böhm, M. Topf, W. Kriegseis, W. Burkhardt, I. Dirnstorfer, S. Rösel, B. Farangis, B. Meyer, A. Hoffmann *et al.*, J. Appl. Phys. **88**, 1811 (2000).
[117]K. Saarinen, T. Laine, S. Kuisma, J. Nissilä, P. Hautojärvi, L. Dobrzynski, J. M. Baranowski, K. Pakula, R. Stepniewski, M. Wojdak, A. Wysmolek, T. Suski, M. Leszczynski, I. Grzegory, and S. Porowski, Phys. Rev. Lett. **79**, 3030 (1997).
[118]F. Tuomisto and I. Makkonen, Rev. Mod. Phys. **85**, 1583 (2013).
[119]B. Raghothamachar, Y. Liu, H. Peng, T. Ailihumaer, M. Dudley, F. S. Shahedipour-Sandvik, K. A. Jones, A. Armstrong, A. A. Allerman, J. Han, H. Fu, K. Fu, and Y. Zhao, J. Cryst. Growth **544**, 125709 (2020).
[120]W. Willoughby, M. Zvanut, and M. Bockowski, J. Appl. Phys. **125**, 075701 (2019).
[121]R. Pässler, J. Appl. Phys. **96**, 715 (2004).
[122]A. Armstrong, A. R. Arehart, D. Green, U. K. Mishra, J. S. Speck, and S. A. Ringel, J. Appl. Phys. **98**, 053704 (2005).
[123]K. Kanegae, H. Fujikura, Y. Otoki, T. Konno, T. Yoshida, M. Horita, T. Kimoto, and J. Suda, Appl. Phys. Lett. **115**, 012103 (2019).
[124]S. Wu, X. Yang, H. Zhang, L. Shi, Q. Zhang, Q. Shang, Z. Qi, Y. Xu, J. Zhang, N. Tang, X. Wang, W. Ge, K. Xu, and B. Shen, Phys. Rev. Lett. **121**, 145505 (2018).
[125]M. Reshchikov, M. Vorobiov, O. Andrieiev, K. Ding, N. Izyumskaya, V. Avrutin, A. Usikov, H. Helava, and Y. Makarov, Sci. Rep. **10**, 1 (2020).
[126]D. V. Lang, J. Appl. Phys. **45**, 3023 (1974).
[127]P. Mooney, in *Defects in Semiconductors*, edited by M. Stavola (Academic Press, London, 1998), Chap. 2, pp. 93–146.
[128]C. E. Dreyer, J. L. Lyons, A. Janotti, and C. G. Van de Walle, Appl. Phys. Expr. **7**, 031001 (2014).
[129]G. Cassabois, P. Valvin, and B. Gil, Nat. Photonics **10**, 262 (2016).
[130]J. Pan, J. Cordell, G. J. Tucker, A. C. Tamboli, A. Zakutayev, and S. Lany, Adv. Mater. **31**, 1807406 (2019).
[131]N. L. Adamski, D. Wickramaratne, and C. G. Van de Walle, J. Mater. Chem. C **8**, 7890 (2020).
[132]M. S. Haseman, B. A. Noesges, S. Shields, J. S. Cetnar, A. N. Reed, H. A. Al-Atabi, J. H. Edgar, and L. J. Brillson, Appl. Phys. Lett. Mater. **8**, 081103 (2020).
[133]N. L. Adamski, C. E. Dreyer, and C. G. Van de Walle, Appl. Phys. Lett. **115**, 232103 (2019).
[134]Y. Taniyasu, M. Kasu, and T. Makimoto, Nature **441**, 325 (2006).
[135]A. Szabó, N. T. Son, E. Janzén, and A. Gali, Appl. Phys. Lett. **96**, 192110 (2010).
[136]C. Stampfl and C. G. Van de Walle, Phys. Rev. B **65**, 155212 (2002).
[137]B. E. Gaddy, Z. Bryan, I. Bryan, R. Kirste, J. Xie, R. Dalmau, B. Moody, Y. Kumagai, T. Nagashima, Y. Kubota, T. Kinoshita, A. Koukitu, Z. Sitar, R. Collazo, and D. L. Irving, Appl. Phys. Lett. **103**, 161901 (2013).
[138]Q. Yan, A. Janotti, M. Scheffler, and C. G. Van de Walle, Appl. Phys. Lett. **105**, 111104 (2014).
[139]T. Roy, M. Tosun, J. S. Kang, A. B. Sachid, S. B. Desai, M. Hettick, C. C. Hu, and A. Javey, ACS Nano **8**, 6259 (2014).
[140]K. Hirama, Y. Taniyasu, H. Yamamoto, and K. Kumamura, Appl. Phys. Lett. **116**, 162104 (2020).
[141]R. H. Wentorf, J. Chem. Phys. **36**, 1990 (1962).
[142]O. Mishima, J. Tanaka, S. Yamaoka, and O. Fukunaga, Science **238**, 181 (1987).
[143]T. Taniguchi, S. Koizumi, K. Watanabe, I. Sakaguchi, T. Sekiguchi, and S. Yamaoka, Diam. Relat. Mater. **12**, 1098 (2003).
[144]L. Weston, D. Wickramaratne, and C. G. Van de Walle, Phys. Rev. B **96**, 100102R (2017).
[145]D. A. Evans, A. G. McGlynn, B. M. Towlson, M. Gunn, D. Jones, T. E. Jenkins, R. Winter, and N. R. J. Poolton, J. Phys. Condens. Matter **20**, 075233 (2008).
[146]K. Chen, B. Song, N. K. Ravichandran, Q. Zheng, X. Chen, H. Lee, H. Sun, S. Li, G. A. G. Udalamatta Gamage, F. Tian, Z. Ding, Q. Song, A. Rai, H. Wu, P. Koirala, A. J. Schmidt, K. Watanabe, B. Lv, Z. Ren, L. Shi, D. G. Cahill, T. Taniguchi, D. Broido, and G. Chen, Science **367**, 555 (2020).
[147]L. Weston, D. Wickramaratne, M. Mackoit, A. Alkauskas, and C. G. Van de Walle, Phys. Rev. B **97**, 214104 (2018).
[148]M. Akiyama, K. Kano, and A. Teshigahara, Appl. Phys. Lett. **95**, 162107 (2009).
[149]F. Perjeru, X. Bai, M. Ortiz-Libreros, R. Higgins, and M. Kordesch, Appl. Surf. Sci. **175–176**, 490 (2001).

[150]H. A. Al-Brithen, A. R. Smith, and D. Gall, Phys. Rev. B **70**, 045303 (2004).
[151]Y. Kumagai, N. Tsunoda, and F. Oba, Phys. Rev. Appl. **9**, 034019 (2018).
[152]B. R. Pamplin, J. Cryst. Growth **26**, 239 (1974).
[153]P. C. Quayle, E. W. Blanton, A. Punya, G. T. Junno, K. He, L. Han, H. Zhao, J. Shan, W. R. L. Lambrecht, and K. Kash, Phys. Rev. B **91**, 205207 (2015).
[154]D. Skachkov, A. Punya Jaroenjittichai, L.-Y. Huang, and W. R. L. Lambrecht, Phys. Rev. B **93**, 155202 (2016).
[155]N. L. Adamski, Z. Zhu, D. Wickramaratne, and C. G. Van de Walle, J. Appl. Phys. **122**, 195701 (2017).
[156]N. L. Adamski, Z. Zhu, D. Wickramaratne, and C. G. Van de Walle, Appl. Phys. Lett. **114**, 032101 (2019).